crystals

MDPI

Article

Ultrafast Laser-Induced Crystallization of Lead Germanate Glass

Sergey V. Lotarev *, Alexey S. Lipatiev, Tatiana O. Lipateva, Elena V. Lopatina and Vladimir N. Sigaev

Department of Chemical Technology of Glass and Sitalls, Mendeleev University of Chemical Technology, Miusskaya Sq. 9, Moscow 125047, Russia; lipatievas@muctr.ru (A.S.L.); t.lipateva@muctr.ru (T.O.L.); ellopa@muctr.ru (E.V.L.); vsigaev@muctr.ru (V.N.S.)

* Correspondence: slotarev@muctr.ru

Abstract: Laser-induced space-selective crystallization of glass enabling the growth of continuous crystal-in-glass architectures consisting of non-centrosymmetric phases with functional properties is promising, including single-crystal waveguides for the development of integrated optical circuits. In this study, femtosecond laser direct writing of crystalline lines inside lead germanate glass with the composition close to $Pb_5Ge_3O_{11}$ has been demonstrated. The growth of crystalline lines by the .moving focused laser beam required the preliminary growth of a seed crystal by the fixed beam. Confocal Raman spectroscopy revealed the precipitation of ferroelectric $Pb_5Ge_3O_{11}$, which, under certain exposure conditions, could be accompanied by precipitation of the metastable lead germanate phase. Depending on the laser beam parameters, either bilateral growth providing split, horseshoe-shaped morphology of the crystal cross-section, or centered growth resulting in elongated, elliptical cross-section shape occurred. The obtained results are of interest for the fabrication of ferroelectric $Pb_5Ge_3O_{11}$-based crystal-in-glass waveguides.

Keywords: space-selective crystallization; lead germanate glass; femtosecond laser; direct laser writing; $Pb_5Ge_3O_{11}$

check for updates

Citation: Lotarev, S.V.; Lipatiev, A.S.; Lipateva, T.O.; Lopatina, E.V.; Sigaev, V.N. Ultrafast Laser-Induced Crystallization of Lead Germanate Glass. *Crystals* **2021**, *11*, 193. https://doi.org/10.3390/cryst11020193

Academic Editor: Bertrand Poumellec
Received: 16 January 2021
Accepted: 9 February 2021
Published: 18 February 2021

Publisher's Note: MDPI stays neutral with regard to jurisdictional claims in published maps and institutional affiliations.

Copyright: © 2021 by the authors. Licensee MDPI, Basel, Switzerland. This article is an open access article distributed under the terms and conditions of the Creative Commons Attribution (CC BY) license (https://creativecommons.org/licenses/by/4.0/).

1. Introduction

Controlled crystallization of glasses providing surface or bulk precipitation of functional crystalline phases is a well-known method for the development of novel functional materials [1]. In the two recent decades, progress in laser technology and laser-assisted microfabrication methods gave rise to numerous studies of laser-induced space-selective crystallization of glass and growth of crystalline architectures in glass by direct laser writing, which have been recently reviewed by Komatsu and Honma [2]. These methods open the way to the fabrication of 2D and 3D components of integrated optical circuits in glass matrix which obtain functional properties of crystals such as high second-order susceptibility, linear electrooptic effect, ferroelectricity, etc. This could make glasses a cost-effective and technologically simpler alternative to single crystals as basic material for integrated photonic devices.

The basic principle of the method is spatially confined absorption of the focused laser beam energy in the irradiated material, producing local heat accumulation and a temperature rise sufficient for nucleation and growth of the target crystalline phase. While the application of continuous-wave lasers requires linear absorption of glass at the laser wavelength and is favorable for surface crystallization, lasers emitting ultrashort pulses with extremely high peak power give a unique opportunity for space-selective modification and heating of inner parts of transparent materials due to the nonlinear nature of absorption limited to the nearest vicinity of the beam waist [3]. Since femtosecond pulses possessing the peak power sufficient to launch nonlinear absorption can have much smaller pulse energy than pico- or nanosecond pulses with the same peak power, they provide more precise micromodification of transparent materials and better controlled thermal effect finely tunable by variation of the pulse energy and repetition rate. In particular,

femtosecond-laser direct writing (FLDW) enables the fabrication of 3D crystalline architectures in the inside of glasses including continuous single-crystal tracks with waveguiding properties [4,5].

The most favorable case for laser-induced growth of continuous crystalline architectures in glass is the precipitation of phases which possess glass-forming properties and thus can be precipitated in glass of the same or similar chemical composition. In this case, crystalline architectures can be grown without a significant composition shift in the surrounding glass and thus are less limited in size and shape. Among these phases, non-centrosymmetric crystals with high or noticeable second-order optical susceptibility such as $LnBGeO_5$ (Ln = La, Sm) [4–8], β-BaB_2O_4 [9], $Ba_2TiSi_2O_8$ [10–12], $Ba_2TiGe_2O_8$ [10], and some others attract wide interest in terms of laser-induced crystal growth in glass. Moreover, the glass-forming ability of these phases facilitates their laser-induced amorphization, thus opening an opportunity for reversible space-selective crystallization [13]. However, some crystals possessing glass-forming composition and interesting functional properties have been out of the scope of these studies so far. In particular, the binary PbO–GeO_2 system has a vast glass-forming region from 0 mol.% to about 75 mol.% PbO [14] including ferroelectrics $PbGe_4O_9$ [15] and $Pb_5Ge_3O_{11}$ [16] which can be precipitated in lead germanate glasses [17–22]. $Pb_5Ge_3O_{11}$ is a ferroelectric phase with trigonal symmetry and Curie temperature at 177 °C, congruently melting at 737 °C and having a space group P3 at room temperature [16,17]. It has attractive pyroelectric properties with a pyroelectric coefficient of 10–45 nC/(cm^2K) and a high pyroelectric figure of merit [23] and was easily precipitated in lead germanate glass of the similar composition [17,19,22].

In the present study, we investigated the possibility and conditions of space-selective crystallization of lead germanate glass similar to the ferroelectric $Pb_5Ge_3O_{11}$ phase in chemical composition by the femtosecond laser beam and analyzed the phases precipitated under the laser exposure by confocal Raman spectroscopy.

2. Materials and Methods

A conventional melt-quenching technique similar to that earlier used to produce lead germanate glasses in our laboratory [20] was applied for glass synthesis. Chemically pure Pb_3O_4 and GeO_2 were taken at the ratio corresponding to $5PbO{\cdot}3GeO_2$ composition, i.e., the stoichiometry of $Pb_5Ge_3O_{11}$ crystal, and well mixed together to prepare the batch calculated to produce 30 g of glass. Melting of the batch was performed in a platinum crucible in an electric furnace with SiC heaters at 1000 °C for 0,5 h. The melt was quenched by pouring on a steel plate and pressing by another plate to the thickness of ~2 mm. The fabricated glass sample was bright-yellow and transparent. It had no visible crystalline inclusions but contained some bubbles. It was cut into several pieces which were polished to ~1 mm thick plane-parallel plates for experiments on direct laser writing. Differential thermal analysis (DTA) of a 10 mg solid piece of the fabricated glass was performed using NETZSCH STA 449 F3 Jupiter®simultaneous thermal analyzer (NETZSCH Holding, Selb, Bayern, Germany) at 10 K/min heating rate. D2 Phaser (Bruker AXS Inc., Madison, WI, USA) diffractometer was used for X-ray diffraction analysis (XRD).

A regeneratively amplified femtosecond laser Pharos SP (Light Conversion Ltd. Vilnius, Lithuania) emitting pulses with a variable duration from 180 fs to 10 ps at an adjustable repetition rate up to 1 MHz at the wavelength of 1030 ± 2 nm was used as a source of laser light for micromodification of the studied samples. In the present study, the pulse duration was always set to 180 fs. The beam quality was characterized by M^2 ~ 1.2. The laser beam was focused into the sample using an Olympus LCPLN50X-IR microscope objective (N.A. = 0.65) at a depth of 100 μm in the air, which gave an actual modification depth of about 0.19 mm due to the refraction of glass. The corresponding refractive index can be therefore roughly estimated as ~1.9. Under these conditions, the calculated beam waist diameter is approximately 1.2 μm. It should be mentioned that spherical aberration is considerable at this focusing depth, and the outermost parts of the beam were expected to be focused up to ~0.22 mm under the glass surface, though their impact in

the modification is moderate because most of the Gaussian beam power is concentrated near the center of its cross-section. In this context, the calculated waist diameter should be regarded as a lower limit of the actual value. The sample was positioned by a 3-coordinate air-bearing motorized translation stage (Aerotech ABL 1000, Aerotech Inc., Pittsburgh, PA, USA) synchronized with the laser. A layout of the setup can be found in [24]. The laser-induced modification of the sample could be visually controlled in-situ by a Retiga 3000 charge-coupled device (CCD) camera (Teledyne QImaging, Surrey, BC, Canada). A simplified layout of the setup is shown in Figure 1.

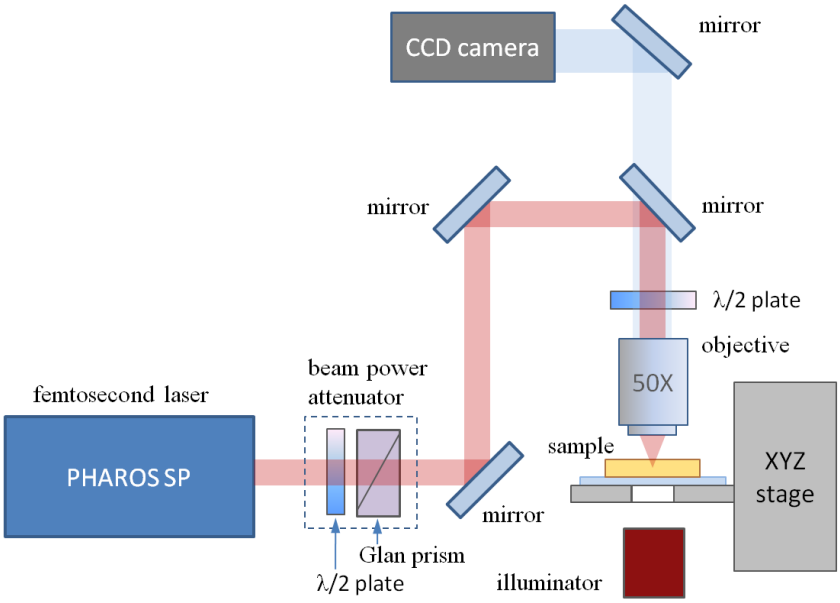

Figure 1. A simplified layout of the direct laser writing setup.

An Olympus BX51 (Japan) polarizing optical microscope was used for visualization of the laser-induced modifications in glass. Observation in crossed polarizers was used to reveal birefringent areas inside the sample. Micro-Raman spectra of starting glass and the laser-written tracks were acquired by means of NTEGRA Spectra confocal Raman spectrometer (NT-MDT Co., Moscow, Russia) in back-scattering geometry under the excitation with a "blue" line (488 nm) of the argon-ion laser focused by Mitutoyo MPlan 100X microscope objective (Japan) into a beam spot with a size of ~0.8 μm. Crosscuts of the samples were made to perform Raman mapping of the cross-section of the laser-written tracks. The acquired Raman spectrum can be considered valid, starting from the wavenumber of ~80 cm^{-1}, as at lower wavenumbers the signal was blocked by the notch filter. The spectral resolution was 1 cm^{-1}.

3. Results

3.1. Crystallization Properties of the Studied Glass

Figure 2a shows the DTA curve of the as-quenched glass under study. The glass transition temperature T_g, temperatures of the onset (T_{x1}), and the maximum (T_{cr1}) of the first exothermic peak are, respectively, 355 °C, 457 °C, and 464 °C. The second exothermic peak is characterized by T_{x2} = 588 °C and T_{cr2} = 599 °C and is much weaker than the first one. The determined values are somewhat higher than those reported for $5PbO{\cdot}3GeO_2$ glass by Lan, et al. [19] (T_g = 335 °C, T_{x1} = 427 °C, T_{cr1} = 427 °C, T_{x1} = 481 °C, T_{cr1} = 490 °C), and Sigaev, et al. [20] (T_g = 333 °C, T_{cr1} = 427 °C, T_{cr1} = ~520 °C). One piece of glass was heat-treated in the electric furnace at 460 °C for 1 h in order to study the crystalline phase precipitating at the first exothermal peak. The XRD pattern of this sample (Figure 2b) conforms well with the XRD pattern of the phase earlier reported to precipitate under heat-treatment at the temperature of the first exothermic peak in $5PbO{\cdot}3GeO_2$ glass [19] which

was shown to be a metastable hexagonal crystalline phase transforming into ferroelectric $Pb_5Ge_3O_{11}$ at higher temperature [17–19]. It was considered to be either $Pb_3Ge_2O_7$ [17] or a metastable form of $Pb_5Ge_3O_{11}$ [18,19]. The second exothermic peak was assigned to the transformation of the metastable phase to stable $Pb_5Ge_3O_{11}$ [17–20]. It can be assumed that the increase of the characteristic temperatures relative to the earlier data indicates the shift of the chemical composition of glass to a lower content of PbO, which could be caused by the evaporation of Pb during melting. On this assumption, the linear extrapolation of the compositional dependence of T_g an T_{cr1} in the range of 58–65 mol.% PbO [17] gives a rough estimation of the actual composition of synthesized glass as 53–54 mol.% PbO.

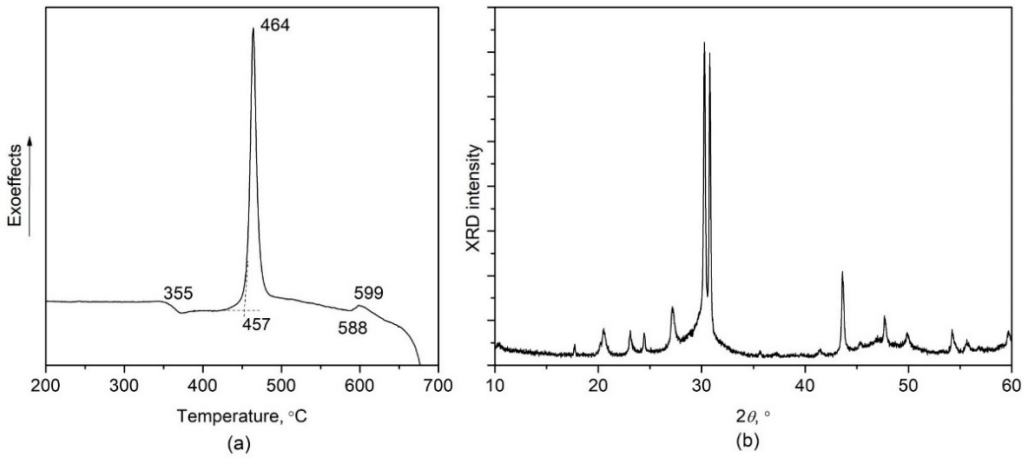

Figure 2. (**a**) DTA curve of the as-quenched glass sample; (**b**) XRD pattern of the glass sample heat-treated at 460 °C for 1 h.

3.2. Laser-Induced Crystallization

Experiments on the FDLW were performed over a wide range of the pulse energy, the pulse repetition rate, and the scanning speed and showed that, similar to lanthanum borogermanate [8,25] lithium niobium silicate [26], and some other glasses, writing crystalline tracks by the moving laser beam requires preliminary growth of a seed crystal by the fixed laser beam. The laser exposure at various pulse energy and repetition rate revealed the favorable pulse energy range of 70–120 nJ (hereafter values measured at the sample surface) at the repetition rate of 500 kHz for fast nucleation and growth of the seed crystal. This pulse energy range corresponds to $(3.4–5.9)\cdot10^{13}$ W/cm^2 peak laser intensity in the focal point. Under these conditions, the incubation time necessary for the appearance of a microcrystal varied from a few seconds to half a minute. Green light of SHG is typically a convenient real-time visual indicator of the appearance of a non-centrosymmetric microcrystal in the area being exposed to the focused femtosecond IR laser beam. However, due to the substantial absorption by yellow lead germanate glass, only a slight SHG signal could be observed. Thus, the detection of microcrystals was performed *in situ* after turning the laser beam off.

When the conditions of the FDLW of continuous crystalline tracks were found, one track was used as a seed and the following tracks were written starting from different points of this seed track perpendicular to its orientation. Laser-written crystalline lines could be easily distinguished from amorphous tracks due to noticeable birefringence visualized in crossed polarizers (Figure 3). Writing in two passes including a first pass at high speed to fabricate a tapered crystal, and a second pass at a slightly reduced speed to extend it into a single-crystal line of arbitrary length, was earlier suggested for the laser-induced growth of $LaBGeO_5$ tracks in lanthanum borogermanate glass [4]. In the case of lead germanate glass, two-pass writing also improved the quality and visual homogeneity of the crystalline tracks. Figure 3 shows examples of the crystalline tracks written at various pulse repetition rates from 200 kHz to 500 kHz. At every pulse repetition rate, there was an optimal pulse energy range providing crystal growth. The higher the pulse repetition rate, the lower the

pulse energy required for laser writing the homogeneous crystalline track. Too high a pulse energy evidently caused the melting of the seed crystal, which prevented further growth of the crystalline line.

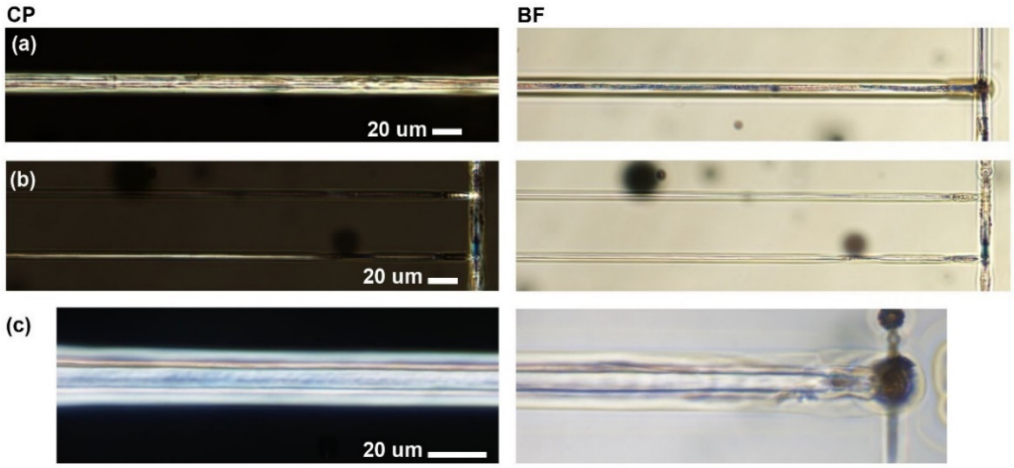

Figure 3. Bright-field (BF) and cross-polarized (CP) optical images of the top-view of the tracks written in lead germanate glass in two passes by the beam at the pulse energy, repetition rate and writing speed of, respectively: (**a**) 170 nJ, 250 kHz, 30 μm/s (1st pass) + 15 μm/s (2nd pass), (**b**) 60 nJ, 500 kHz, 30 μm/s (1st pass) + 20 μm/s (2nd pass, upper track) or 18 μm/s (2nd pass, lower track) (**c**) 250 nJ, 200 kHz, 30 μm/s (1st pass) + 20 μm/s (2nd pass).

3.3. Confocal Raman Spectroscopy of the Laser-Induced Crystalline Tracks

Confocal Raman spectroscopy was used to obtain information about the crystalline phase precipitating under the laser beam. In order to obtain a higher contribution of the crystalline tracks into the registered Raman scattering signal and to analyze the spatial distribution of the crystal inside the track, each sample was cut in the plane perpendicular to the tracks. Their cross-sections were exposed, polished, and studied by optical microscopy. Raman mapping was carried out for three of them. These tracks are further referred to as Track I (Figure 3a), Track II (Figure 3b, lower track), and Track III (Figure 3b, upper track). Raman spectra acquired in certain points on the cross-sections of these tracks are shown in Figure 4, as well Raman spectra of as-quenched glass (Figure 4, curve 1), heat-treated at the temperatures of the first exothermic peak (Figure 4, curve 2) and above the second exothermic peak (Figure 4, curve 8).

Examination of Raman spectra registered in different points of the cross-section of Track I revealed patterns presumably corresponding to two different crystalline phases. The Raman spectrum of the phase located in the upper part of the cross-section (Figure 4, curve 3) is quite similar to the spectrum of glass crystallized by heat-treatment at 460 °C for 1 h (Figure 4, curve 2) and containing the metastable hexagonal phase (Figure 2b). The Raman spectrum acquired in the lower part of the cross-section corresponds well with that of glass crystallized by heat-treatment at 670 °C for 1 h (Figure 4, curve 8) and with Raman spectra of polycrystalline trigonal ferroelectric $Pb_5Ge_3O_{11}$ [20] (Figure 4, curve 8) [21], and earlier spectroscopic data on $Pb_5Ge_3O_{11}$ single crystal [27–29]. Unlike in Track I, only Raman spectra similar to those of the ferroelectric phase were revealed in crystallized parts of the cross-sections of Tracks II and III (Figure 4, curves 5, 6).

Figure 5 shows cross-polarized optical images and Raman maps of the cross-sections of the discussed tracks. According to the visible distribution of the birefringent areas in the cross-section of Track I (Figure 5a, line I), it included two separated crystallized areas including a horseshoe-shaped area enveloping the center of the track from top and both sides and a triangular area in the bottom. A strong narrow Raman band with a maximum at 96 cm^{-1} is the most pronounced peak in the spectrum of the trigonal $Pb_5Ge_3O_{11}$ in the registered range and therefore was used for detection of this phase in the mapping of the

maximal peak value in the range 90–110 cm^{-1} (Figure 5b) and the steepness of the slope in the range 110–120 cm^{-1} (Figure 5c). Since the absolute intensity of Raman scattering in the mentioned range depends on the intensity of other low-frequency vibration bands and some instrumental factors, steepness of the slope in the range 110–120 cm^{-1} enables more accurate distinguishing of the growth of the peak at 96 cm^{-1} and so Figure 5c gives a more relevant representation of the location of this phase. In order to locate the metastable hexagonal phase, a minor peak centered at 454 cm^{-1} characteristic for this phase was used for its mapping. Similar to the previous case, the steepness of the slope (Figure 5e) appears to be a better distinctive feature for visualization of the growth of this peak than the maximal peak intensity in this spectral range (Figure 5d). It should be mentioned that a negative sign is assigned to rising slopes in the applied software and so the steeper low-frequency slope and consequently the stronger peak at 454 cm^{-1} is represented by the darker areas of the map in Figure 5e.

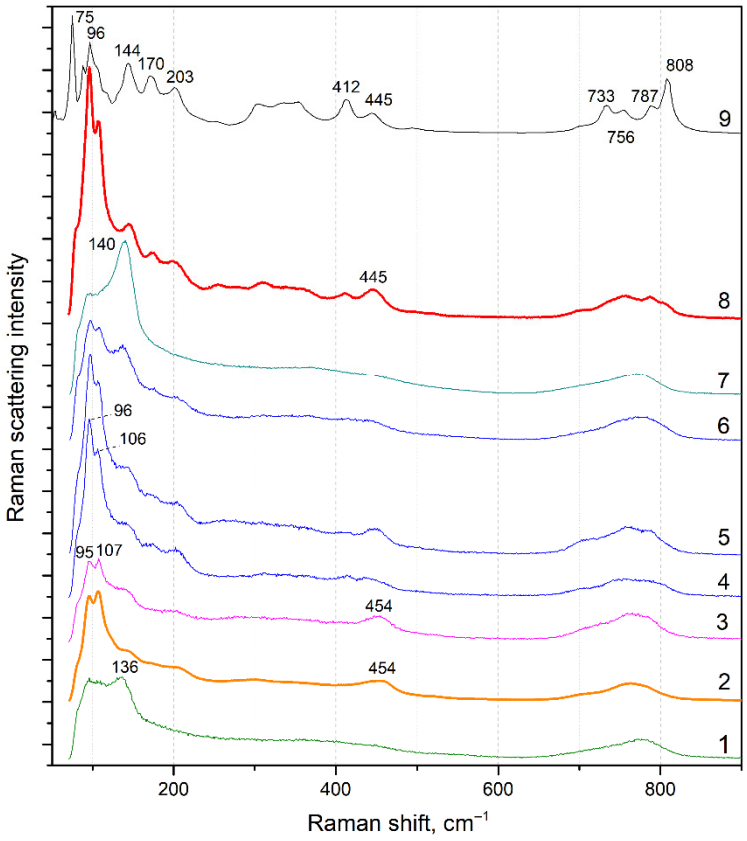

Figure 4. Nonpolarized Raman spectra of starting glass (**1**), glass heat-treated at 460 °C for 1 h (**2**), top (**3**), and bottom (**4**) crystallized areas of the cross-section of track I, crystallized area of the cross-section of track II (**5**), crystallized area of the cross-section of track III (**6**), top area of the of the cross-section of track III (**7**), glass heat-treated at 670 °C for 1 h (**8**), Raman spectrum of the polycrystalline $Pb_5Ge_3O_{11}$ sample divided by the Bose–Einstein thermal factor presented by Sigaev, et al. [20] (**9**).

Raman maps of the cross-sections of Tracks II and III give the crystalline phase distribution other than in Track I. In these tracks, the stable trigonal $Pb_5Ge_3O_{11}$ is the only or dominant phase and is concentrated in the central area of the cross-section, being somewhat shifted to the top in the case of Track III. The crystallized part of the cross-section is substantially elongated along the beam but is not split into partially or fully separated fragments. The Raman spectrum registered in Track 3 (Figure 4, curve 6) includes a weak band with the maximum at 451 cm^{-1} which is in the intermediate position between the maxima characteristic for the stable ferroelectric (445 cm^{-1}) and metastable (454 cm^{-1})

phases and may indicate the residue of the latter. Due to the relatively small size of the crystal area in the Track III compatible with the spatial resolution of the spectrometer for transparent media, it was poorly distinguished by the confocal scheme, and its spectrum (Figure 4, curve 6) contains a much stronger component related to surrounding glass (for instance, a peak at ~140 cm^{-1}), as compared to the Track II (Figure 4, curve 5).

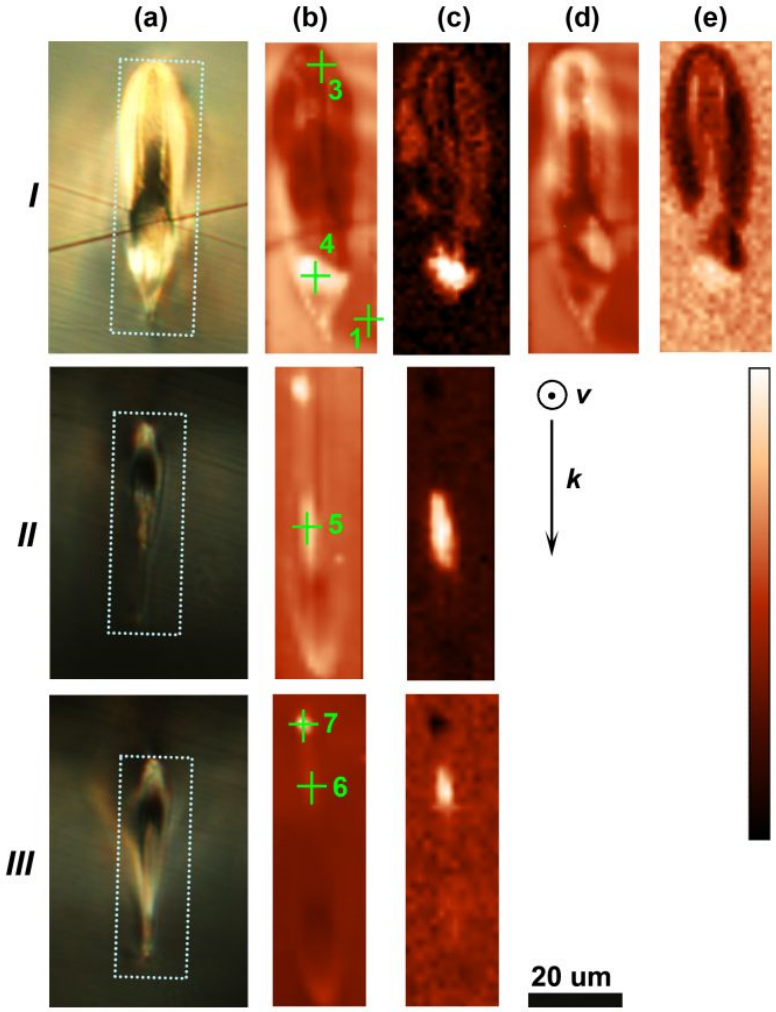

Figure 5. Cross-polarized optical images (**a**) and pseudo-color Raman maps (**b–e**) of the cross-sections of the tracks I, II, III: Brightness of the maps shows a peak value in the ranges 90–110 cm^{-1} (**b**) and 450–470 cm^{-1} (**d**), steepness of the spectral curve in the ranges 110–120 cm^{-1} (**c**) and 440–454 cm^{-1} (**e**); dotted frames show areas of Raman mapping; green crosses indicate points of acquisition of the Raman spectra with corresponding numbers given in Figure 4; k and v show, respectively, propagation and scanning directions of the writing laser beam; the scale bar is for optical images.

Another interesting feature of the Raman spectra registered in the amorphous area of Tracks II and III is a substantial growth of the peak at 136 cm^{-1} together with the shift of its maximum to 140 cm^{-1} observed in the top and bottom edges of the cross-section. It can be evidence of an increased PbO content because it likely has the same origin as the strong band at the similar position in Raman spectra of binary lead borate glasses which was assigned to symmetrical vibrations of [PbO_4] trigonal bipyramids [30]. The growth of the relative intensity and the high-frequency shift of the maximum of this line was shown to correlate with an increase in the PbO content in lead germanate glasses [20].

4. Discussion

The FDLW in the studied lead germanate glass is shown to enable the growth of continuous crystalline lines consisting of the $Pb_5Ge_3O_{11}$ regardless the revealed difference of the glass composition with the stoichiometry of the crystal. Depending on laser exposure conditions, growth of the stable trigonal phase can be accompanied by the precipitation of the metastable hexagonal phase which evidently appears in the regions with lower average temperature insufficient to induce its transformation to the stable ferroelectric form of $Pb_5Ge_3O_{11}$ during the time until the laser-induced heat is dissipated by surrounding glass. Some minor difference between the acquired Raman spectra assigned to the stable $Pb_5Ge_3O_{11}$ from the spectra reported for ferroelectric $Pb_5Ge_3O_{11}$ [20,28,29] such as a much weaker band at 808 cm^{-1} or less pronounced bands in the range of 320–420 cm^{-1} can be related either to an incomplete transformation from the metastable phase or to the oriented character of laser-induced crystallization taking into account that these Raman components are expressed to various extents depending on the orientation of the crystal axes and the excitation beam. The issues of orientation and the microcrystalline structure of the laser-written crystal lines require further investigation involving electron microscopy and electron backscatter diffraction analysis.

The complicated split shape of the crystalline part of the cross-section revealed in Track I containing a horseshoe-shaped fragment is typical for the bilateral crystal growth described in detail for lanthanum borogermanate glass [31]. However, in the case of the lead germanate glass under study, the variation of the laser beam parameters appears to allow for the control of the cross-section shape and for avoiding the lateral character of crystal growth. Under the applied focusing conditions, the growth of a centered continuous crystalline track consisting of stable $Pb_5Ge_3O_{11}$ and having a nearly 10 μm × 2 μm sized cross-section was realized at the relatively small average beam power of 30 mW and the small pulse energy of 60 nJ, though at the high pulse repetition rate of 500 kHz, providing the stronger thermal effect.

The assumption on Pb ion migration from the central part to the top and the bottom of the cross-section of the laser-modified tracks made based on Raman spectra conforms to principles of ultrafast-laser-induced ion migration due to thermal diffusion (Soret effect) which typically causes an increase in the concentration of monovalent and bivalent cations in the periphery of the regions modified by the focused laser beam [32]. An increased PbO content locally increases the crystallization ability and can additionally promote lateral crystallization for two reasons: first, it brings the glass composition close to the composition of the precipitating crystal in the case of glass under study, and second, it decreases the connectivity of the glass network, glass transition temperature and the viscosity, which is known to facilitate rearrangement of the cations and to increase the crystallization ability [33]. A similar trend of the crystallization ability under the local increase in the modifier oxide content was demonstrated in experiments on femtosecond laser-induced crystallization of lanthanum borogermanate glass [34]. The increase in the PbO content in the top part of the cross-section of the laser-written track could also be the factor favorable for centered growth of the crystal such as observed in Tracks II and III as it would make the crystallization ability in the top part of the cross-section higher than in the lateral parts. However, it should be further verified by the elemental microanalysis methods.

5. Conclusions

In summary, conditions of femtosecond laser direct writing of continuous crystalline lines inside lead germanate glass possessing a composition close to $Pb_5Ge_3O_{11}$ stoichiometry with a certain shift to higher GeO_2 content were revealed. The growth of crystalline lines by the moving focused laser beam required the preliminary growth of a seed crystal by the fixed beam. The laser-written crystalline lines consisted of trigonal ferroelectric $Pb_5Ge_3O_{11}$ but, under certain exposure conditions, could also include the metastable hexagonal lead germanate phase which is known to transform into stable ferroelectric $Pb_5Ge_3O_{11}$ under heat-treatment. Similar to earlier reported laser-writing of $LaBGeO_5$ crystal-in-glass lines,

two-pass writing enabled the substantial improvement of continuity and homogeneity of the crystalline lines as compared to single-pass writing in lead germanate glass.

Depending on the laser exposure parameters, either bilateral growth providing a split, horseshoe-shaped morphology of the crystal cross-section, or centered growth resulting in elongated, elliptical cross-section shape occurred. The case of centered growth is favorable for the application of the laser-written crystalline tracks as channel waveguides. However, the possibility of writing highly-oriented single-crystalline lines which is important for elaboration of low-loss crystal-in-glass waveguides based on $Pb_5Ge_3O_{11}$ phase requires further investigation of the orientation and microcrystalline structure of the laser-written crystal lines by means of high-resolution electron microscopy and electron backscatter diffraction analysis.

Author Contributions: Conceptualization, V.N.S. and S.V.L.; methodology, S.V.L. and A.S.L.; validation, S.V.L., T.O.L. and E.V.L.; investigation, A.S.L., E.V.L. and T.O.L.; writing—original draft preparation, S.V.L.; writing—review and editing, A.S.L., T.O.L. and V.N.S.; visualization, E.V.L.; supervision, V.N.S.; project administration, S.V.L.; funding acquisition, S.V.L. All authors have read and agreed to the published version of the manuscript.

Funding: This research was funded by Mendeleev University of Chemical Technology, grant number 026-2020.

Acknowledgments: We acknowledge N.V. Golubev for performing X-ray diffraction analysis for this study.

Conflicts of Interest: The authors declare no conflict of interest.

References

1. Komatsu, T. Design and control of crystallization in oxide glasses. *J. Non-Cryst. Solids* **2015**, *428*, 156–175. [CrossRef]
2. Komatsu, T.; Honma, T. Laser patterning and growth mechanism of orientation designed crystals in oxide glasses: A review. *J. Solid State Chem.* **2019**, *275*, 210–222. [CrossRef]
3. Gattass, R.R.; Mazur, E. Femtosecond laser micromachining in transparent materials. *Nat. Photon* **2008**, *2*, 219–225. [CrossRef]
4. Stone, A.; Jain, H.; Dierolf, V.; Sakakura, M.; Shimotsuma, Y.; Miura, K.; Hirao, K.; Lapointe, J.; Kashyap, R. Direct laser-writing of ferroelectric single-crystal waveguide architectures in glass for 3D integrated optics. *Sci. Rep.* **2015**, *5*, 10391. [CrossRef] [PubMed]
5. Lipatiev, A.S.; Lipateva, T.O.; Lotarev, S.V.; Okhrimchuk, A.G.; Larkin, A.S.; Presnyakov, M.Y.; Sigaev, V.N. Direct Laser Writing of $LaBGeO_5$ Crystal-in-Glass Waveguide Enabling Frequency Conversion. *Cryst. Growth Des.* **2017**, *17*, 4670–4675. [CrossRef]
6. Gupta, P.; Jain, H.; Williams, D.B.; Honma, T.; Benino, Y.; Komatsu, T. Creation of Ferroelectric, Single-Crystal Architecture in $Sm_{0.5}La_{0.5}BGeO_5$ Glass. *J. Am. Ceram. Soc.* **2007**, *91*, 110–114. [CrossRef]
7. Stone, A.; Sakakura, M.; Shimotsuma, Y.; Stone, G.; Gupta, P.; Miura, K.; Hirao, K.; Dierolf, V.; Jain, H. Directionally controlled 3D ferroelectric single crystal growth in $LaBGeO_5$ glass by femtosecond laser irradiation. *Opt. Express* **2009**, *17*, 23284–23289. [CrossRef]
8. Stone, A.; Sakakura, M.; Shimotsuma, Y.; Miura, K.; Hirao, K.; Dierolf, V.; Jain, H. Unexpected influence of focal depth on nucleation during femtosecond laser crystallization of glass. *Opt. Mater. Express* **2011**, *1*, 990–995. [CrossRef]
9. Nishii, A.; Shinozaki, K.; Honma, T.; Komatsu, T. Morphology and orientation of β-BaB_2O_4 crystals patterned by laser in the inside of samarium barium borate glass. *J. Solid State Chem.* **2015**, *221*, 145–151. [CrossRef]
10. Honma, T.; Komatsu, T.; Benino, Y. Patterning of c-axis-oriented $Ba_2TiX_2O_8$ (X = Si, Ge) crystal lines in glass by laser irradiation and their second-order optical nonlinearities. *J. Mater. Res.* **2008**, *23*, 885–888. [CrossRef]
11. Zhu, B.; Dai, Y.; Ma, H.; Zhang, S.; Qiu, J. Direct writing Eu^{3+}-doped $Ba_2TiSi_2O_8$ crystalline pattern by femtosecond laser irradiation. *J. Alloy. Compd.* **2008**, *460*, 590–593. [CrossRef]
12. Lipatiev, A.S.; Moiseev, I.A.; Lotarev, S.V.; Lipateva, T.O.; Presnyakov, M.Y.; Fedotov, S.S.; Sigaev, V.N. Growth of Fresnoite Single Crystal Tracks Inside Glass Using Femtosecond Laser Beam Followed by Heat Treatment. *Cryst. Growth Des.* **2018**, *18*, 7183–7190. [CrossRef]
13. Lotarev, S.V.; Lipatiev, A.S.; Lipateva, T.O.; Fedotov, S.S.; Naumov, A.S.; Moiseev, I.A.; Sigaev, V.N. Ultrafast-laser vitrification of laser-written crystalline tracks in oxide glasses. *J. Non-Cryst. Solids* **2019**, *516*, 1–8. [CrossRef]
14. Mazurin, O.V.; Streltsina, M.V.; Shvaiko-Shvaikovskaya, T.P. *Properties of Glasses and Glassforming Melts, Reference Book*; Part 2; Nauka: Leningrad, Russia, 1993. (In Russian)
15. Venevtsev, Y.N.; Bush, A.A.; Shashkov, A.Y.; Chetchkin, V.V.; Hertsen, N.P.; Stefanovich, S.Y.; Rannev, N.V. Lead tetragermanate crystals: Polymorphism, crystal structure and properties. *Ferroelectrics* **1982**, *45*, 203–209. [CrossRef]
16. Iwasaki, H. Ferroelectric and optical properties of $Pb_5Ge_3O_{11}$ and its isomorphous compound $Pb_5Ge_2SiO_{11}$. *J. Appl. Phys.* **1972**, *43*, 4907–4915. [CrossRef]

17. Hasegawa, H.; Shimada, M.; Koizumi, M. Phase relations and crystallization of glass in system PbO-GeO_2. *J. Mater. Sci.* **1973**, *8*, 1725–1730. [CrossRef]
18. Nassau, K.; Shiever, J.; Joy, D.; Glass, A. The crystallization of vitreous and metastable $Pb_5Ge_3O_{11}$. *J. Cryst. Growth* **1977**, *42*, 574–578. [CrossRef]
19. Lan, G.-X.; Sun, H.-Y.; Yin, Z.-Y.; Wang, J.-Y.; Wang, H.-F. Raman Spectroscopic Study of Amorphous $Pb_5Ge_3O_{11}$ and Its Crystallization. *Phys. Status Solidi* **1991**, *164*, 39–44. [CrossRef]
20. Sigaev, V.N.; Gregora, I.; Pernice, P.; Champagnon, B.; Smelyanskaya, E.N.; Aronne, A.; Sarkisov, P.D. Structure of lead germanate glasses by Raman spectroscopy. *J. Non-Cryst. Solids* **2001**, *279*, 136–144. [CrossRef]
21. Scavini, M.; Tomasi, C.; Speghini, A.; Bettinelli, M. Stable and Metastable Phases within the GeO_2-Rich Part of the Binary PbO–GeO_2 System. *J. Mater. Synth. Process.* **2001**, *9*, 93–102. [CrossRef]
22. Stefanovich, S.Y.; Sigaev, V.N. Application of the optical second harmonic generation method in the study of the crystal-lization of noncetrosymmetric phases in glasses. *Glass Phys. Chem.* **1995**, *21*, 253–262.
23. Viennois, R.; Kityk, I.; Majchrowski, A.; Żmija, J.; Mierczyk, Z.; Papet, P. Influence of Cr^{3+} doping on the enhanced dielectric and nonlinear optical features of pyroelectric $Pb_5Ge_3O_{11}$ single crystals. *Mater. Chem. Phys.* **2018**, *213*, 461–471. [CrossRef]
24. Lotarev, S.; Fedotov, S.; Lipatiev, A.; Presnyakov, M.; Kazansky, P.; Sigaev, V. Light-driven nanoperiodical modulation of alkaline cation distribution inside sodium silicate glass. *J. Non-Cryst. Solids* **2018**, *479*, 49–54. [CrossRef]
25. Lipateva, T.O.; Lotarev, S.V.; Lipatiev, A.S.; Kazansky, P.G.; Sigaev, V.N. Formation of crystalline dots and lines in lanthanum borogermanate glass by the low pulse repetition rate femtosecond laser. *Photonics Devices Syst. VI* **2015**, *9450*, 945018. [CrossRef]
26. Cao, J.; Lancry, M.; Brisset, F.; Mazerolles, L.; Saint-Martin, R.; Poumellec, B. Femtosecond Laser-Induced Crystallization in Glasses: Growth Dynamics for Orientable Nanostructure and Nanocrystallization. *Cryst. Growth Des.* **2019**, *19*, 2189–2205. [CrossRef]
27. Soni, R.K.; Jain, K.P. High pressure raman scattering in $Pb_5Ge_3O_{11}$. *Pramana* **1986**, *27*, 707–712. [CrossRef]
28. Müller-Lierheim, W.; Suski, T.; Otto, H.H. Factor group analysis of the Raman spectrum of $Pb_5Ge_3O_{11}$. *Phys. Status Solidi (b)* **1977**, *80*, 31–41. [CrossRef]
29. Lockwood, D.J.; Hosea, T.J.; Taylor, W. The complete Raman spectrum of paraelectric and ferroelectric lead germanate. *J. Phys. C: Solid State Phys.* **1980**, *13*, 1539–1553. [CrossRef]
30. Zahra, A.-M.; Zahra, C.; Piriou, B. DSC and Raman studies of lead borate and lead silicate glasses. *J. Non-Cryst. Solids* **1993**, *155*, 45–55. [CrossRef]
31. Stone, A.; Sakakura, M.; Shimotsuma, Y.; Miura, K.; Hirao, K.; Dierolf, V.; Jain, H. Femtosecond laser-writing of 3D crystal architecture in glass: Growth dynamics and morphological control. *Mater. Des.* **2018**, *146*, 228–238. [CrossRef]
32. Fernandez, T.; Sakakura, M.; Eaton, S.; Sotillo, B.; Siegel, J.; Solis, J.; Shimotsuma, Y.; Miura, K. Bespoke photonic devices using ultrafast laser driven ion migration in glasses. *Prog. Mater. Sci.* **2018**, *94*, 68–113. [CrossRef]
33. Wagstaff, F.E. Crystallization and Melting Kinetics of Cristobalite. *J. Am. Ceram. Soc.* **1969**, *52*, 650–654. [CrossRef]
34. McAnany, S.D.; Veenhuizen, K.J.; Kiss, A.M.; Thieme, J.; Nolan, D.A.; Aitken, B.G.; Dierolf, V.; Jain, H. Evolution of glass structure during femtosecond laser assisted crystallization of $LaBGeO_5$ in glass. *J. Non-Cryst. Solids* **2021**, *551*, 120396. [CrossRef]